AGU PUBLICATIONS

JGR

Journal of Geophysical Research: Oceans

RESEARCH ARTICLE

10.1002/2015JC011359

**Key Points:**
- Chukchi Sea subsurface chlorophyll layers are sensitive to seasonal water mass changes
- Nutrient-rich Winter Water replaces nutrient-poor Chukchi Summer Water causing biomass to decrease
- Subsurface chlorophyll layers contribute 17–67% of net biomass, higher than previous estimates

**Correspondence to:**
K. I. Martini,
kmartini@uw.edu

**Citation:**
Martini, K. I., P. J. Stabeno, C. Ladd, P. Winsor, T. J. Weingartner, C. W. Mordy, and L. B. Eisner (2016), Dependence of subsurface chlorophyll on seasonal water masses in the Chukchi Sea, *J. Geophys. Res. Oceans*, *121*, 1755–1770, doi:10.1002/2015JC011359.

Received 30 SEP 2015
Accepted 8 FEB 2016
Accepted article online 12 FEB 2016
Published online 16 MAR 2016



# Dependence of subsurface chlorophyll on seasonal water masses in the Chukchi Sea

**Kim I. Martini[1,2], Phyllis J. Stabeno[1], Carol Ladd[1], Peter Winsor[3], Thomas J. Weingartner[3], Calvin W. Mordy[1,2], and Lisa B. Eisner[4]**

[1]Pacific Marine Environmental Laboratory, Seattle, Washington, USA, [2]Joint Institute for the Study of the Atmosphere and Ocean, University of Washington, Seattle, Washington, USA, [3]Institute of Maine Science, School of Fisheries and Ocean Science, University of Alaska Fairbanks, Fairbanks, Alaska, USA, [4]Alaska Fisheries Science Center, Seattle, Washington, USA

**Abstract** During the late summer, phytoplankton in the northeastern Chukchi Sea are typically found in subsurface layers. These layers and their sensitivity to local changes in hydrography and nutrient concentrations are characterized by combining data from a high-resolution towed sampling platform with traditional shipboard observations. The replacement of surface meltwater and deeper nutrient-rich Chukchi Winter Water by northward flowing nutrient-poor Chukchi Summer Water and Remnant Winter Water leads to a net decrease in biomass and smaller phytoplankton. Between 17 and 67% of phytoplankton biomass is contained within the subsurface layers. This estimate is nearly twice as high as previous estimates from sparser shipboard data and suggests subsurface phytoplankton contribute significantly to the net biomass in the Chukchi Sea in late summer.

## 1. Introduction

The Chukchi Sea is home to a unique and highly productive ecosystem that is subject to intense seasonal variability. The unique physical environment affects organisms from lower to higher trophic levels and hosts an annual series of phytoplankton blooms [*Hill and Cota*, 2005; *Wassmann and Reigstad*, 2011]. The spring-summer biological cycle begins with algal growth at the marginal ice edge, or in some areas under the ice *Arrigo et al*. [2008], that transition to open water blooms with the retreat of sea ice [*Wassmann and Reigstad*, 2011; *Arrigo et al*., 2012]. As nutrients are depleted at the surface, subsurface chlorophyll maxima (SCM) develop in late summer and early fall as phytoplankton descend to utilize higher nutrient concentrations at depth [*Cota et al*., 1996; *Codispoti et al*., 2005; *Tremblay et al*., 2008; *Martin et al*., 2010; *Ardyna et al*., 2013; *Brown et al*., 2015; *Coupel et al*., 2015]. Secondary summer surface blooms triggered by mixing events that transport nutrients to the surface also occur during the late summer and early fall (July–October), but are not as common [*Wang et al*., 2005; *Pabi et al*., 2008]. After the spring phytoplankton bloom, the largest chlorophyll concentrations are found within the SCM, nearly an order of magnitude larger than surface concentrations [e.g., *Hill and Cota*, 2005; *Martin et al*., 2010; *Popova et al*., 2010; *Lowry et al*., 2015]. A significant fraction of late summer primary production is also estimated to occur within the SCM [*Ardyna et al*., 2013; *Hill et al*., 2013]. Understanding the physical processes that drive the SCM and control its extent is important to understand the role and contribution of phytoplankton in the Chukchi Sea ecosystem in late summer.

The hydrography of the Central Chukchi Sea is determined by the annual cycle of ice growth and melt, and by the northward advection of water from the Bering Strait. In fall, ice formation and accompanying brine rejection leads to the formation of cold ($T < -1°C$) and salty ($S > 32$ psu) Chukchi Winter Water (CWW) which pools at the bottom of this shallow sea. As the winter progresses, this bottom water becomes saltier with additional brine rejection [*Woodgate et al*., 2005]. In spring, there is a dramatic change in stratification due to sea ice melt, which forms a layer of cold ($T < 2°C$), fresh ($S < 30$ psu) meltwater (MW) at the surface. The surface MW layer persists after the sea ice retreats northward, until it is eventually replaced by warmer ($T > 2°C$) and saltier ($S > 30$ psu) Chukchi Summer Water (CSW) originating in the Bering Sea or from waters modified locally on the Chukchi shelf [*Gong and Pickart*, 2015]. It flows northward through the Chukchi Sea and into the Arctic, forced by the pressure head between the Arctic and Pacific Oceans [*Coachman and Aagaard*, 1966; *Stigebrandt*, 1984; *Weingartner et al*., 2005; *Gong and Pickart*, 2015]. Fronts occur at the surface as the warmer CSW pushes the colder MW northward [*Paquette and Bourke*, 1974; *Paquette and Bourke*,

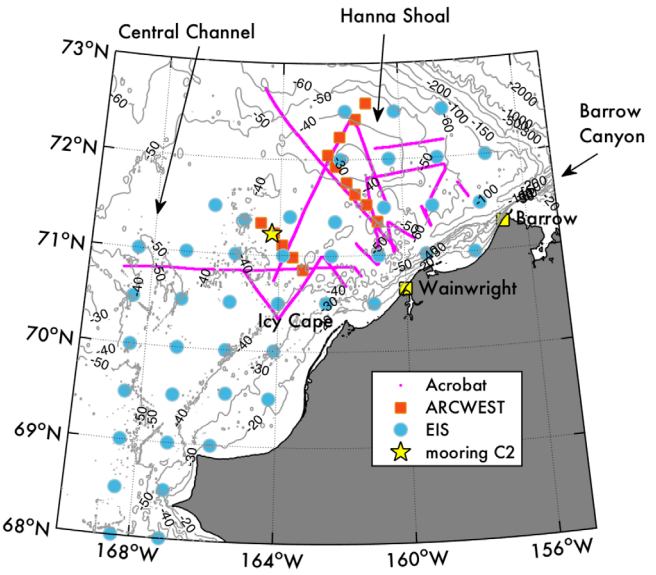


**Figure 1.** Map of the Central Chukchi Sea shelf with bathymetric contours (gray), showing the locations of the Acrobat transects (pink lines), shipboard CTD stations during the ARCWEST (red squares) and Arctic Eis (blue circles) cruises, the PMEL mooring C2 (yellow star), and relevant geographical landmarks (yellow squares).

1981; *Lu et al*., 2015]. Deeper CWW is replaced by Remnant Winter Water (RWW) formed earlier in the Bering that is slightly warmer ($-1°C < T < 0°C$) due to mixing with surface summer waters [*Gong and Pickart*, 2015]. Unlike the surface layer, there is no definitive front between Chukchi Winter Water and Remnant Winter Water due to the relatively small changes in horizontal density. When comparing RWW and CWW to the upper layer, we treat both as the same water mass, collectively referring to them as Winter Water (WW). It should be noted that the temperature and salinity ranges used here to define the water masses differ from those of *Coachman et al*. [1975].

The well-mixed bottom and surface layers are separated by a sharp pycnocline, creating a two-layer, salinity-stratified fluid in the Central Chukchi Sea in late summer. This stratified system limits vertical mixing and inhibits the exchange of nutrients, salt, and heat between the upper and lower layers and supports the development of the SCM as a balance between light and nutrient availability. Nitrate is the limiting nutrient in the Arctic basin and shelf seas [*Sakshaug*, 2004; *Tremblay et al*., 2006] and the nitracline depth is directly tied to water column structure. Previous studies have shown that phytoplankton growth and SCM depth are correlated with the availability of light and the vertical structure of nutrient concentrations [*Martin et al*., 2010; *McLaughlin and Carmack*, 2010; *Wassmann and Reigstad*, 2011; *Brown et al*., 2015; *Coupel et al*., 2015; *Lowry et al*., 2015]. On the Chukchi shelf, the nitracline is located between high nutrient concentrations in the deep WW and low nutrients in surface CSW and MW layers and affects SCM depth and biomass [*Brown et al*., 2015; *Coupel et al*., 2015]. Nitrate usage in the Chukchi Sea likely has downstream effects in the Arctic, as Winter Water originating in the Chukchi Sea is an important source of nitrate to the deep Arctic basin [*Walsh et al*., 1989]. Nutrient consumption by biological processes in the Chukchi Sea can limit the amount of nutrients entering the Arctic basin [*Cooper et al*., 1999], perhaps affecting biological processes there.

Phytoplankton biomass and primary production are likely to change in response to changes in the physical environment [*Wassmann and Reigstad*, 2011]. Production may decrease in the Chukchi as the input of nutrient-poor freshwater from rivers and ice melt increases [*Yun et al*., 2014] and in the Canada Basin as the nitracline deepens with recent freshening [*McLaughlin and Carmack*, 2010; *Coupel et al*., 2015]. On the other hand, annual production may increase due to increased upwelling on the northern edge of the Chukchi shelf [*Carmack and Chapman*, 2003; *Pickart et al*., 2013; *Brugler et al*., 2014]. The impact of a longer ice-free season on primary production is variable, ranging from positive [*Arrigo and Dijken*, 2011; *Pabi et al*., 2008] to negative [*Bélanger et al*., 2013] in the Arctic Ocean and inconclusive in the Beaufort Sea [*Martin et al*., 2010]. Over the Chukchi shelf, changes in primary production and nitracline depth have not been observed; however, high spatial and temporal variability in primary production suggest these results should be regarded with caution [*Coupel et al*., 2015]. These changes are likely to cascade across trophic levels, as Arctic marine ecosystems are sensitive to changes in primary production [*Grebmeier et al*., 2006]. In particular, the largest increases in primary production have been occurring on the Arctic shelves [*Arrigo and Dijken*, 2011], suggesting the greatest changes to ecosystems may be occurring in locations such as the Chukchi Sea.

We will show here that the depth of the SCM in late summer is sensitive to seasonal changes in hydrography. The SCM is spatially variable, but the extent and prevalence of subsurface chlorophyll *a* patches have not been well characterized due to the limited horizontal sampling resolution of shipboard observations. Using new data from a high-resolution towed profiling vehicle (Acrobat), the central Chukchi Sea SCM is

mapped during August–September 2013. Combining traditional shipboard physical, biological, and chemical data, we will investigate how seasonal changes in hydrography, stratification, and nutrient distribution affect subsurface phytoplankton biomass and composition in the late summer.

## 2. Data and Methods

By combining Acrobat data and traditional shipboard data from two cruises, we explore how changes in hydrography affect the extent and depth of the SCM. Each data set has specific advantages. Acrobat data are used to create high-resolution hydrographic maps and improve estimates of phytoplankton distributions (based on chlorophyll *a* fluorescence) using >5000 profiles along the 1600 km ship track, but provide no chemical or optical data. Shipboard data include nutrients, oxygen, Photosynthetically Active Radiation (PAR), and discrete chlorophyll samples in addition to hydographic data, but sparser horizontal sampling does not consistently capture small-scale variability. Lastly, data from a mooring cluster deployed offshore of Icy Cape (Figure 1) are used to examine currents that advect seasonal hydrographic features affecting the SCM.

### 2.1. Acrobat Data

From 6 to 19 September 2013, multiple high-resolution hydrographic transects were made in the northeast Chukchi Sea from the R/V Norseman using a Sea Sciences Acrobat. This towed vehicle was used to map the horizontal and vertical extent of water masses and the SCM. Only transects on the shallow Chukchi shelf are discussed here, although the Acrobat did pass over upper Barrow Canyon. The sampling region is shown in Figure 1.

The Acrobat is a winged instrument platform that cycles between the surface and 80 m as it is towed behind a ship traveling at speeds of 5–6 knots. It was equipped with a SeaBird 43 FastCAT CTD (temperature, conductivity, and pressure) and a Wetlabs EcoPUCK optical sensor (chlorophyll *a*, colored dissolved organic matter (CDOM), and turbidity). Profiles were collected every 300 m over 1600 km for a total of >5000 profiles. The CTD data were corrected for thermistor thermal response, time lag due to the physical separation of the temperature and conductivity sensors, and conductivity sensor thermal lag following *Johnson et al*. [2007]. An additional correction was applied to the CTD pressure to account for Acrobat pitch. During descents (ascents), the CTD was tilted so that the pressure sensor was above (below) the temperature and conductivity sensors, causing pressure data to lag (lead) the temperature and conductivity measurements. The EcoPUCK did not have a pressure sensor, so depth was added to the data via interpolation using time stamps generated by the data acquisition computer. Each profile was binned to 0.5 m vertical resolution. Acrobat chlorophyll *a* concentrations were calibrated against a laboratory standard by the manufacturer, but were not calibrated against water samples taken in situ and thus can only be considered a measure of relative concentration.

### 2.2. Shipboard Measurements

Temperature, salinity, chlorophyll *a*, and nutrient data were obtained on two separate cruises: the Arctic Ecosystem Integrated Survey (Arctic Eis) and the Arctic Whale Ecology Study (ARCWEST). The Arctic Eis cruise (7 August 2013 to 6 September 2013) also collected phytoplankton size-structure data. The ARCWEST cruise was conducted 31 August 2013 to 18 September 2013 aboard the F/V Aquila in the Chukchi and Bering Seas, but only data from 31 August to 6 September obtained in the Chukchi Sea are presented here.

Arctic Eis hydrographic and discrete sample data (nutrients, chlorophyll *a*) were collected over the Chukchi Sea shelf at stations spaced ~55 km apart (Figure 1). Sampling started in Bering Strait and moved northward along zonal transects toward the Chukchi shelf break (S. L. Danielson et al., A comparison between late summer 2012 and 2013 water masses, macronutrients, and phytoplankton standing crops in the northern Bering and Chukchi Seas, submitted to *Deep Sea Research, Part II*, 2016). Hydrographic data were collected with a Sea-Bird Electronics Inc. 911plus CTD with dual temperature, conductivity, and oxygen sensors, a Li-Cor 4 pi PAR sensor and a Wetlabs Wet-Star fluorometer. Water samples for nutrients and total chlorophyll were collected at 10 m intervals over the water column, with size-fractionated chlorophyll *a* collected at two of the depths (10 and 30 m). Water samples for nutrients were filtered through 0.45 μm filters, stored at −80°C and later analyzed for dissolved phosphate, silicic acid, nitrate, nitrite, and ammonium using colorometric methods [*Gordon et al*., 1994]. Water samples for chlorophyll were filtered onto GF/F filters (nominal pore size 0.7 μm) for totals and polycarbonate membrane filters (pore size 10 μm) for large

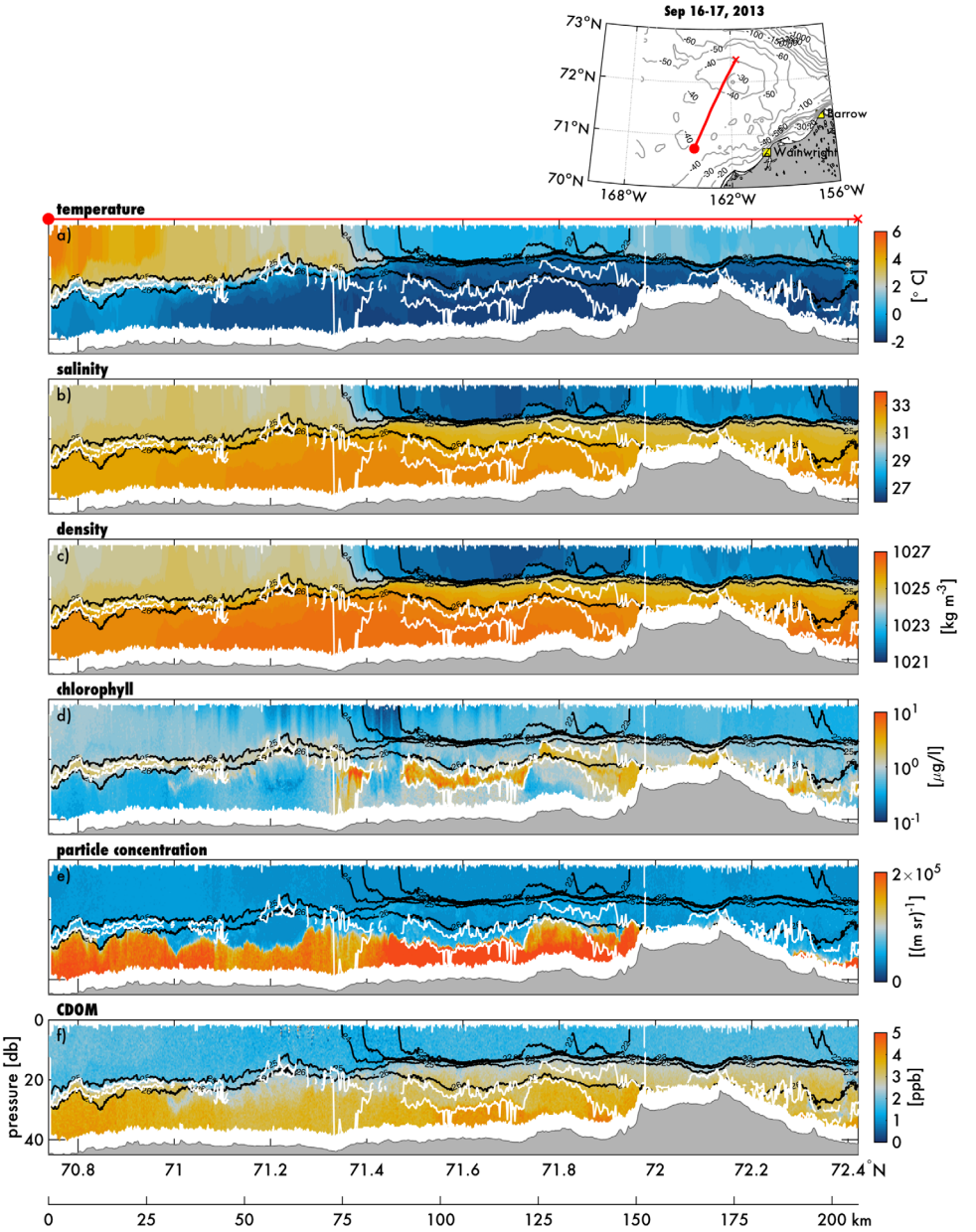


**Figure 2.** South-north cross section of (a) temperature, (b) salinity, (c) potential density, (d) chlorophyll concentration, (e) particle concentration, and (f) colored dissolved organic matter (CDOM) made with the Acrobat profiler on 16–17 September 2013. In each plot, isopycnals are noted in black and the edges of the SCMs in white. The ship track (red) is shown in the map at the top. The red dot indicates the start of the transect, corresponding to the left side of plots and is illustrated for reference in Figure 2a.

size fractions. The filters were stored at −80°C and later processed at a shore-based facility using a benchtop Turner TD-700 fluorometer following standard techniques [*Parsons et al*., 1984].

During the ARCWEST cruise, oceanographic and lower trophic level sampling was conducted along six transect lines. Methods included high-resolution vertical profiling of water properties (including temperature, salinity, chlorophyll *a* fluorescence, PAR, and dissolved $O_2$) to within 4 m of the bottom using a Sea-Bird Electronics 911plus CTD with dual temperature, conductivity, and oxygen sensors. Nutrient (dissolved phosphate, silicic acid, nitrate, nitrite, and ammonium) and chlorophyll samples were collected at discrete depths (0–40 m in 10 m intervals and at the bottom) and frozen at −80°C for analysis at a later date at the NOAA laboratories in Seattle. Dissolved oxygen and salinity samples were taken at every other cast to calibrate the oxygen and conductivity sensors, respectively.

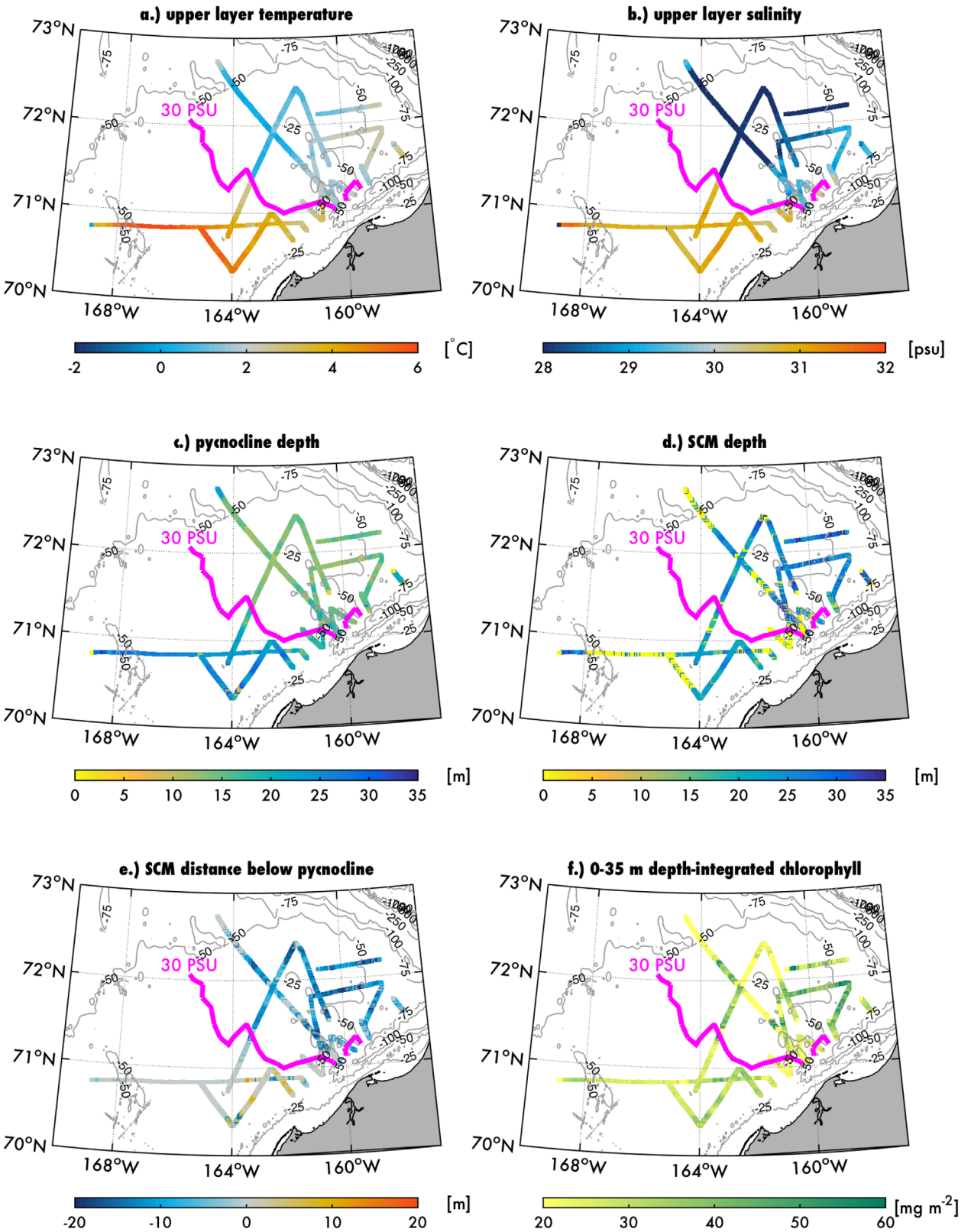


**Figure 3.** Spatial maps of (a) upper layer temperature, (b) upper layer salinity, (c) pycnocline depth, (d) SCM depth, (e) SCM distance below the pycnocline, and (f) depth-integrated chlorophyll fluorescence from Acrobat data. Bathymetric contours are plotted in grey. The interpolated 30 psu salinity contour (magenta line) marks the approximate location of the front between fresh, cold MW in the north and salty, warm CSW in the south. Yellow in Figure 3d means there is no SCM.

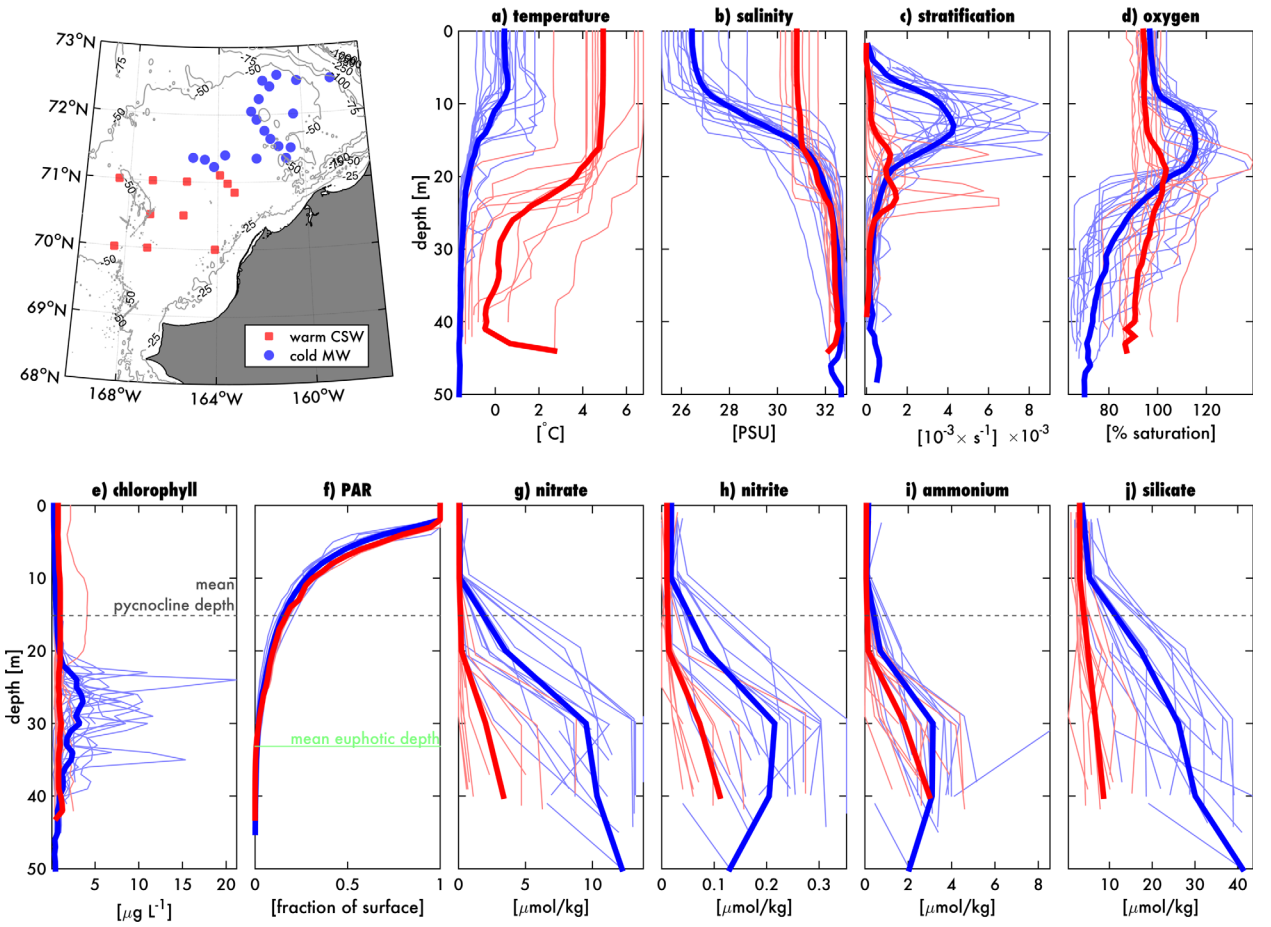


**Figure 4.** Hydrography and nutrients from shipboard (a–f) CTD and (g–j) bottle profiles from 0 to 50 m separated into warm CSW (red) and cold MW profiles (blue). Thin lines are individual casts and thick lines are mean profiles binned onto 1 and 10 m for CTD and bottle casts, respectively. Mean pycnocline depth is noted in gray on Figures 4e–4j and mean euphotic depth in green on Figure 4f.

### 2.3. C2 Mooring

To examine the currents, data from a cluster of two oceanographic moorings spaced 400 m apart and deployed off Icy Cape (71.22°N, 164.25°W) in the northeastern Chukchi Sea from August 2010 to September 2014 were used (Figure 1). An upward-looking 600 kHz RDI ADCP current meter at 36 m measured horizontal water velocities in 5 m bins from 5 to 35 m depth.

### 2.4. Identification of the SCM

Because the SCM is nonsymmetrical, the depth of the SCM is defined here to be the depth of the maximum chlorophyll *a* concentration in each profile. Profiles with maximum chlorophyll *a* concentrations less than 1.39 μg $L^{-1}$ in the Acrobat data and 1.18 μg $L^{-1}$ in the shipboard data are classified as not having a SCM. This threshold corresponds to one standard deviation above the mean chlorophyll concentration for the upper 15 m, which was determined to not contain a SCM.

To estimate the thickness and biomass within the SCM, the upper and lower boundaries of the SCM are defined as the first and last data point in each profile to satisfy two conditions: (1) chlorophyll *a* concentrations above the previous threshold, and (2) the absolute value of the vertical chlorophyll *a* gradient is greater than the mode gradient. These two conditions ensure that the thickness of the SCM is not overestimated due to occasionally large chlorophyll *a* concentrations observed outside of the SCM. Sensitivity testing of the SCM detection algorithm shows that choosing a threshold above the mean chlorophyll *a* concentration in the upper 15 m, 1 μg $L^{-1}$, is sufficient to distinguish SCMs from the "background" phytoplankton profile and yielded similar distributions of SCM thickness and biomass.

**Table 1.** Characteristics of the SCM From Acrobat and Shipboard Data Where There Is MW and CSW[a]

| | ACROBAT | | | Shipboard Data | | |
|---|---|---|---|---|---|---|
| | ALL | MW | CSW | ALL | MW | CSW |
| *Surface Layer Hydrography* | | | | | | |
| Temperature (°C) | | **1.1 ± −0.6** | **4.2 ± 1.1** | | **0.4 ± 0.7** | **4.8 ± 1.2** |
| Salinity (PSU) | | **28.0 ± 0.8** | **30.9 ± 0.3** | | **27.1 ± 0.9** | **30.9 ± 0.4** |
| Phosphate (μmol/kg) | | | | | **0.40 + 0.10** | **0.29 + 0.04** |
| Silicate (μmol/kg) | | | | | 4.36 + 1.81 | 3.306 + 1.18 |
| Nitrate (μmol/kg) | | | | | 0.09 + 0.129 | 0.07 + 0.10 |
| Nitrite (μmol/kg) | | | | | **0.02 + 0.01** | **0.01 + 0.01** |
| Ammonium (μmol/kg) | | | | | **0.14 + 0.09** | **0.07 + 0.06** |
| *Bottom Layer Hydrography* | | | | | | |
| Temperature (°C) | | **−1.2 ± 0.4** | **0.4 ± 1.7** | | **−1.4 ± 0.1** | **0.8 ± 1.9** |
| Salinity (PSU) | | **32.0 ± 0.5** | **32.3 ± 0.3** | | 32.1 ± 0.3 | 32.3 ± 0.3 |
| Phosphate (μmol/kg) | | | | | **1.46 + 0.22** | **0.85 + 0.30** |
| Silicate (μmol/kg) | | | | | **25.76 + 6.84** | **7.35 + 3.20** |
| Nitrate (μmol/kg) | | | | | **8.26 + 2.50** | **2.25 + 2.45** |
| Nitrite (μmol/kg) | | | | | **0.17 + 0.07** | **0.08 + 0.06** |
| Ammonium (μmol/kg) | | | | | 2.43 + 1.18 | 2.14 + 1.17 |
| *SCM Properties* | | | | | | |
| Temperature (°C) | | **−1.4 ± 0.5** | **2.4 ± 1.8** | | −1.5 ± 0.2 | 1.0 ± 3.1 |
| Salinity (PSU) | | **32.3 ± 0.4** | **31.6 ± 0.5** | | 32.5 ± 0.3 | 32.2 ± 0.5 |
| Depth (m) | | **26 ± 4** | **23 ± 6** | | 28 ± 4 | 26 ± 7 |
| Pycnocline depth (m) | | **14 ± 2** | **23 ± 5** | | **13 ± 2** | **19.7 ± 3** |
| Distance below pycnocline (m) | | **−12 ± 4** | **0 ± 6** | | **−15 ± 3** | **−5 ± 6** |
| Thickness (m) | | **6 ± 4** | **6 ± 6** | | **10 ± 6** | **9 ± 8** |
| Maximum chlorophyll *a* (μg/L) | | **3.47 ± 2.81** | **1.83 ± 0.62** | | **5.18 + 2.87** | **1.88 ± 1.19** |
| Depth-integrated chlorophyll (mg/m$^2$) | | **16.62 ± 12.29** | **10.61 ± 9.37** | | 34.00 ± 24.37 | 23.00 ± 27.33 |
| *Biomass* | | | | | | |
| Depth mean chlorophyll *a* (μg/L) | | **0.91 ± 0.34** | **0.87 ± 0.19** | | 1.26 ± 0.50 | 0.97 + 0.69 |
| 0–35 m depth-integrated chlorophyll *a* (mg/m$^2$) | | **29.46 ± 11.47** | **28.65 ± 5.87** | | 43.92 ± 19.43 | 30.86 ± 16.07 |
| Full depth-integrated chlorophyll *a* (mg m$^{-2}$) | 29 ± 9 | 28.65 ± 11.21 | 28.57 ± 5.84 | 39 ± 19 | **51.73 ± 22.89** | **35.57 ± 17.67** |
| SCM percent of total biomass (%) | 39 ± 23 | 46 ± 22 | 31 ± 23 | 56 ± 25 | 60 ± 22 | 40 ± 34 |

[a]Values shown with ±one standard deviation. Bold values show Welch's *t* test *p* values where MW and CSW are the different at the 1% significance level. Surface and bottom values are the mean above and below the pycnocline, respectively. Shipboard chlorophyll *a* concentrations are from fluorometer data calibrated with discrete samples. The depth mean is the average over each profile and SCM depth-integrated values are integrated over the thickness of the SCM.

### 2.5. Biomass Calculations

Fluorometer data are used as a proxy for biomass, as the shipboard water samples were vertically too sparse to accurately resolve the SCM. Biomass estimates made using water samples and in vivo fluorometer data compare fairly well. The shipboard fluorometer mounted on the CTD rosette typically underestimated laboratory estimated chlorophyll *a* concentrations by 25%, but the relationship between the two is linear. The percentage of total biomass within the SCM calculated from the Acrobat fluorometer (39 ± 23%) is well within one standard deviation of shipboard fluorometer estimate (56 ± 25%). While the biomass estimates from the shipboard and Acrobat fluorometers are not accurate, their linear relationship to laboratory samples indicates that they can be used to compare relative concentrations from profile to profile in order to determine (1) geographical changes in biomass and (2) the fractional contribution of the SCM to the total biomass.

## 3. Results and Discussion

### 3.1. Characteristics of the SCM and Hydrography

In late summer 2013 in the central Chukchi Sea, chlorophyll *a* was typically found in 2–40 m thick layers, the center of which ranged in depth from 10 to 40 m. These SCMs occurred over a wide range of horizontal scales, from a series of compact patches as little as 150 m wide to 45 km long sheets (Figure 2).

SCMs were found in nearly all Acrobat transects and 70% of the Acrobat profiles, except for those within 50 km of the coast (not shown) likely due to the presence of the Alaskan Coastal Current (ACC). The ACC is

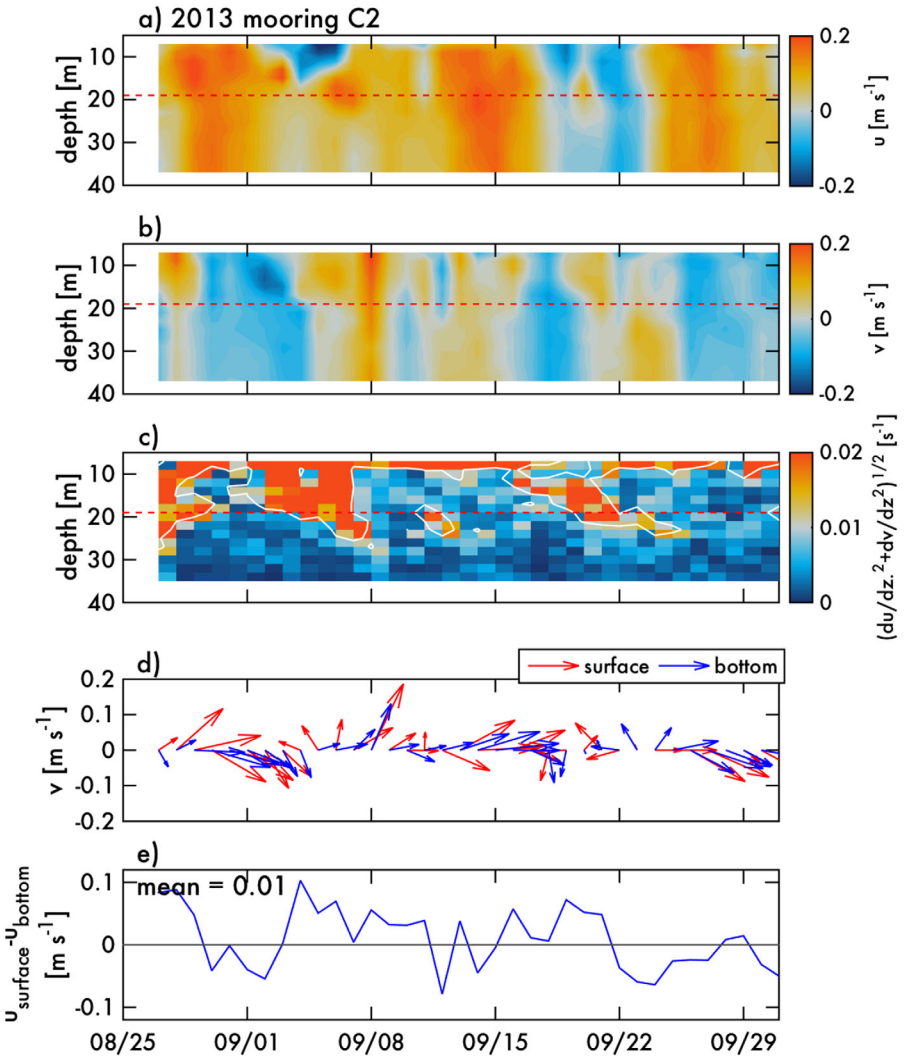


**Figure 5.** ADCP data from mooring C2 from August–September 2013; (a) 2 day low-passed meridional velocity, (b) 2 day low-passed zonal velocity, (c) vertical shear, (d) daily mean velocity in upper (red) and lower (blue) layers, and (e) shear between layers. The dashed horizontal red line at 19 m in Figures 5a–5c represents the boundary between the upper and lower layers.

a coastal current that flows northward along the eastern edge of the Chukchi Sea, through Barrow Canyon and into the Beaufort Sea [*Coachman et al*., 1975; *Woodgate et al*., 2005; *Gong and Pickart*, 2015]. It is comprised of warmer and fresher Alaskan Coastal Water and is weakly stratified and generally low in nutrients [*Codispoti et al*., 2005, 2009; Danielson et al., submitted manuscript, 2016].

In the central Chukchi Sea outside of the influence of the ACC, the depth of the SCM shoals as MW is replaced by CSW. The surface layer was comprised of cold and fresh MW in the northern part of the region and warm and salty CSW in the southern part (Figures 2a and 2b). In the Acrobat transect taken on 16–17 September, the CSW/MW front was located at 71.4°N and both water masses overlay colder and saltier WW.

The variations of SCM depth with hydrography can clearly be seen in the high-resolution meridional transect made with the Acrobat (Figure 2). At the southern end of the transect where there was warm CSW, chlorophyll *a* concentrations were highest in a 5–10 m thick band centered between the 25 and 26 kg $m^{-3}$ isopycnals within the pycnocline. At the northern end of transect under MW, chlorophyll *a* concentrations were highest in a band well below the pycnocline. This pattern (SCM located at the pycnocline where there is CSW and located 10–30 m below the pycnocline under MW) was observed in both the Acrobat tracks (Figure 3) and shipboard data (Figure 4).

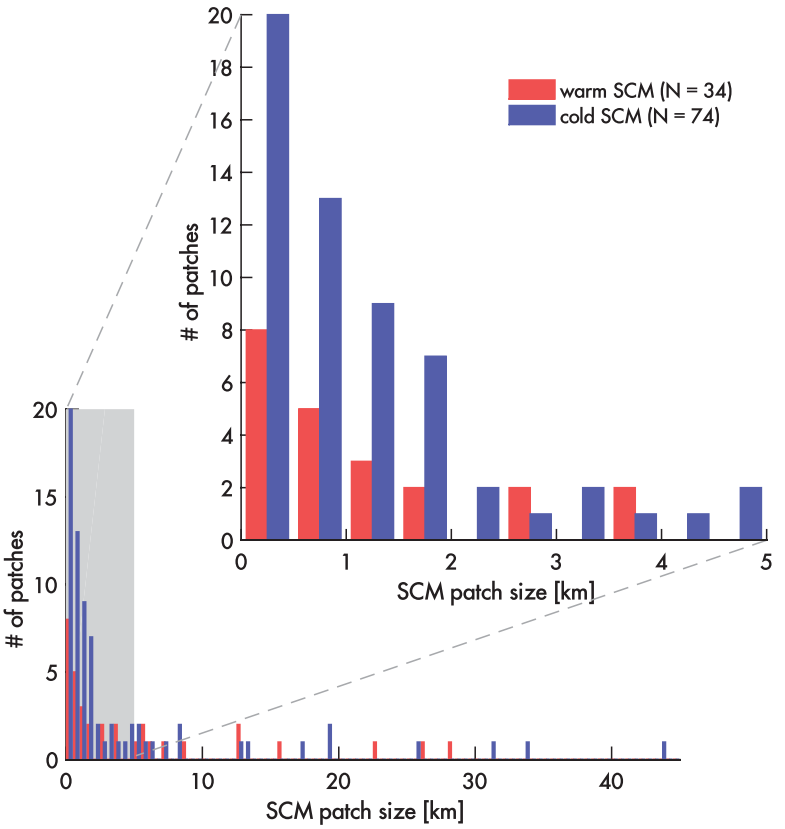


**Figure 6.** Histogram of SCM patch size made from Acrobat data divided into 0.5 km bins, with the 0–5 km size range enlarged (which contains >80% of the patches). There are 34 and 74 distinct SCM patches observed where there is warm CSW (red) and cold MW (blue), respectively.

Mean characteristics of the SCM beneath CSW and MW are quantified using the Acrobat and shipboard data (Table 1). In the Acrobat data, the SCMs were found at 26 m under MW and 23 m where there is CSW, while the pycnocline was found at 14 (MW) and 23 m (CSW) (Table 1), leading to a shoaling of the SCM relative to pycnocline from −12 (MW) to 0 (CSW) m. The deeper CSW pycnocline is attributed to a greater net volume of CSW rather than mechanical deepening by vertical mixing, as salinity is not conserved across the MW/CSW front. The MW SCM was typically located within the bottom CWW layer (mean SCM temperature and salinity: −1.4°C and 32.3 psu) while the CSW SCM was located in the pycnocline (2.4°C and 31.6 psu), leading to significant differences in the hydrographic environment experienced by the phytoplankton. Similarly, in Acrobat surveys from 2012 (not shown), SCMs were observed beneath MW at depth ranges 10–30 m below the pycnocline, with a mean depth of 27.1 ± 8.2 m indicate SCMs occur annually under MW, consistent with previous studies [*Hill et al*., 2005; *Martin et al*., 2010; *Ardyna et al*., 2013; *Questel et al*., 2013].

Estimates from the Acrobat data are generally more robust than shipboard data due to larger sample sizes. In shipboard data, SCMs were observed at most cold MW stations while only at a handful of warm CSW stations, likely due to sparser sampling. Distances between adjacent shipboard stations (∼16–27 and ∼55 km for ARCWEST and Arctic Eis cruises, respectively) were often larger than the width of the SCM patches (mean width ∼3.3 km). However, the shipboard means fall within one standard deviation of the Acrobat means suggesting a similar population is being sampled in each data set.

### 3.2. Currents

Acrobat and shipboard observations present a semisynoptic snapshot of water mass and phytoplankton distributions in the northeastern Chukchi Sea during late summer 2013. However, these distributions change as the net currents flow northward from Bering Strait into the Arctic Ocean, replacing MW with CSW

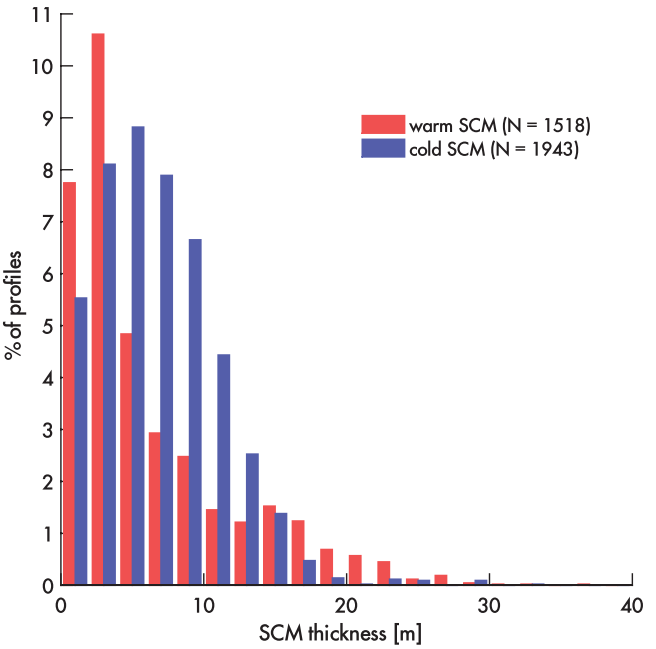


**Figure 7.** Histogram of SCM thickness made from Acrobat data separated in 2 m bins where there is warm CSW (red) and cold MW (blue).

from the south. Observations from the C2 mooring (Figure 1) are used to examine the currents (Figure 5) that drive changes in surface water mass distribution.

While on average flow is northward, reversals due to winds are common [*Weingartner et al.*, 2005]. At C2, average currents above and below 19 m (the average depth of the pycnocline) were generally in the same direction. Mean shear was positive, indicating that the upper layer was moving faster ($\sim$0.13 m $s^{-1}$) than the bottom layer ($\sim$0.10 m $s^{-1}$). Comparisons between the ARCWEST and Acrobat data suggest that the MW/CSW front was advected northward $\sim$25.5 km between 5 and 16 September, at a speed of $\sim$0.03 m $s^{-1}$ (mean surface ADCP velocities were $\sim$0.04 m $s^{-1}$ during this period), likely passing the mooring on 5 September 2013 (Figure 4). Unfortunately, the passage of the MW/CSW front was not observed in the moored data, as the instruments were located near the bottom, well within the bottom WW layer. Satellite ice concentration data indicate that the edge of the ice pack (taken here to be the 50% concentration contour) retreated northward faster than the surface currents ($\sim$0.1 m $s^{-1}$), having passed 73°N on 23 July 2013.

These velocities are similar to annual estimates of 0.05 m $s^{-1}$ [*Woodgate et al.*, 2005] and 0.06–0.07 m $s^{-1}$ (P. J. Stabeno, personal communication, 2015). The transit time for water to flow from the Bering Strait to the front location at 73°N (628 km) is estimated to be 17–20 weeks. A simple calculation assuming the front location only depends on advection (although this is unlikely as the front location is also affected by the timing of sea-ice melt) suggests that the front would have passed through Bering Strait sometime between 23 April and 17 May. Sea ice does not typically retreat from Bering Strait until mid-May, but ice concentration in Bering Strait started to decline on 29 April, consistent with these rough estimates.

### 3.3. SCM Thickness and Extent

While the SCM has been previously detected from shipboard CTD surveys [*Tremblay et al.*, 2008; *Martin et al.*, 2010; *McLaughlin and Carmack*, 2010], the high spatial resolution of the Acrobat data allows a more robust description of SCM extent and thickness and how it relates to other water properties. This high-resolution sampling also provides a first-order effort to quantify the spatial density of chlorophyll *a* in the SCM.

A total of 188 distinct SCM patches were observed in 2013 (Figure 6). The patches ranged in length from 0.15 to 44 km with an average patch length of 3.6 $\pm$ 6.0 km. Patches occupied 48% of the total distance sampled (611 km) indicating there were large gaps between adjacent patches. The thickness of the SCMs ranged from 1 to 38 m with average thickness of 8.4 $\pm$ 6.4 m (Figure 7). Although SCM patch size and thickness are subdivided by surface MW and CSW in Figures 6 and 7, the mean SCM thickness and patch size in these two water masses were not significantly different.

A similar analysis using September 2012 Acrobat data showed SCM patches ranging in length from 0.27 to 27 km, mean patch lengths of 2.1 $\pm$ 3.8 km, and mean SCM thickness of 12.8 $\pm$ 10.3 m. Significantly less distance was covered in 2012 and as a result, fewer SCM patches (53) were observed. More interestingly, only 21% of the September 2012 profiles contained an SCM, suggesting that although less distance was covered, SCM patches were sparser that year and may be indicative of interannual variability.

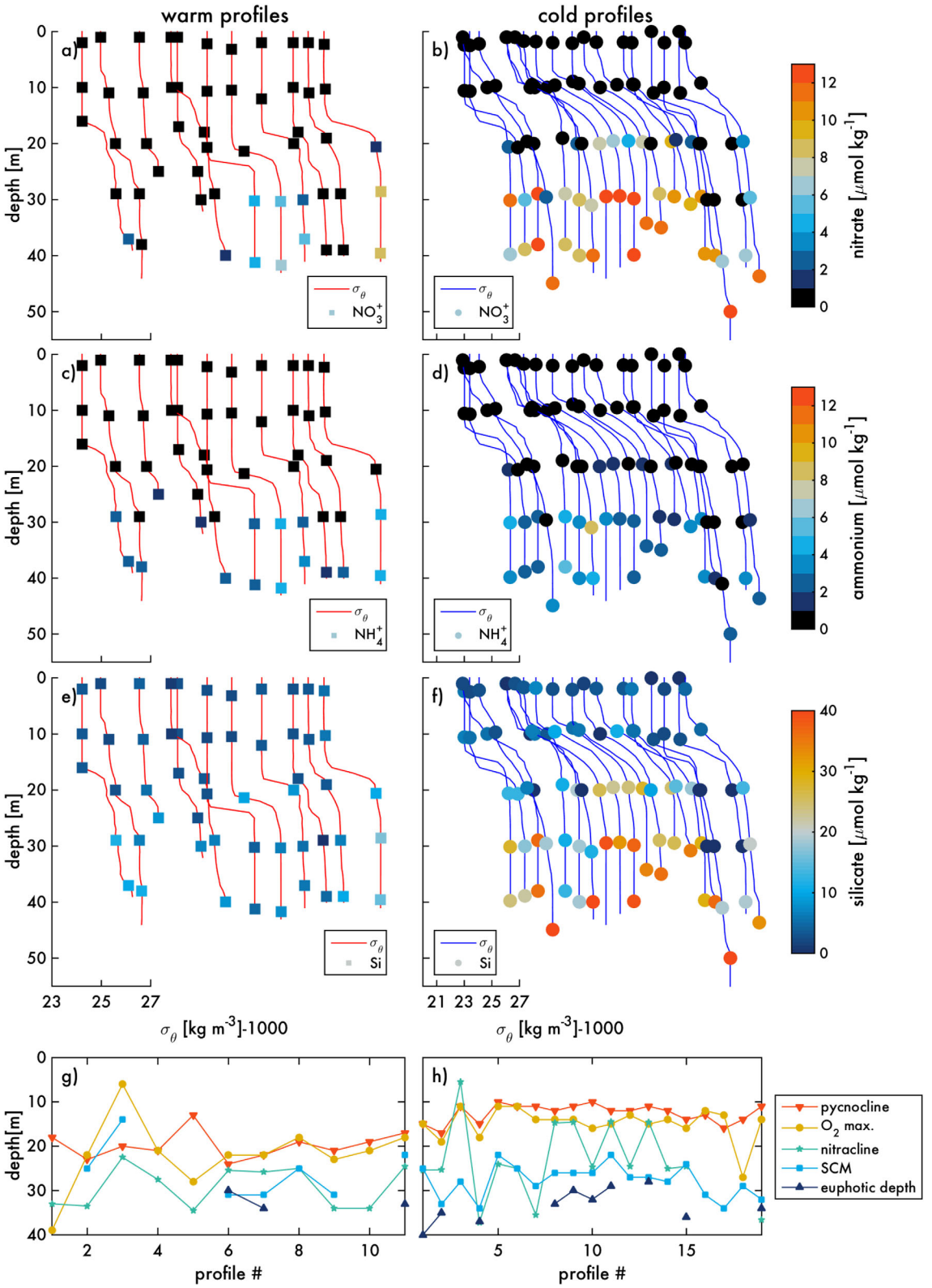


**Figure 8.** Potential density profiles (red/blue lines) with (a and b) nitrate, (c and d) ammonium, and (e and f) silicate concentrations plotted at each sampling depth from shipboard data. (g and h) Comparison of pycnocline depth (red triangles), oxygen maximum depth (yellow circles), nitracline depth (green stars), SCM depth (light blue squares), and euphotic depth (dark blue upward triangles) at each profile. Data are split into (a, c, e, and g) warm and (b, d, f, and h) cold profiles and arranged by latitude, south to north going from left to right and offset by 1 kg $m^{-3}$.

**Table 2.** Oxygen Saturation and Nutrient Concentrations at the Chlorophyll *a* Maximum in the SCM From Shipboard Data[a]

| | MW | CSW |
|---|---|---|
| Oxygen saturation (%) | 86 ± 12 | 96 ± 10 |
| Phosphate (μmol/kg) | **1.35 ± 0.19** | **0.72 ± 0.39** |
| Silicate (μmol/kg) | **24.25 ± 6.29** | **4.65 ± 1.94** |
| Nitrate (μmol/kg) | **7.40 ± 2.40** | **2.04 ± 2.60** |
| Nitrite (μmol/kg) | **0.17 ± 0.07** | **0.06 ± 0.05** |
| Ammonium (μmol/kg) | 1.99 ± 0.59 | 1.47 ± 1.64 |

[a]Bold values show Welch's *t* test *p* values where values in MW and CSW SCM are the different at the 1% significance level.

### 3.4. Nutrients and Light

Late summer SCMs in the Central Chukchi Sea form as a response to nutrient depletion in the surface layer. Here we investigate whether changes in nutrient concentration associated with hydrographic changes impact SCM depth. By late August 2013, the upper water column was depleted of nutrients, i.e., nitrate, nitrite, ammonium, and silicate concentrations were less than 2, 0.1, 1, and 10 μmol $kg^{-1}$, respectively (Figures 4g–4j and Table 1), while below the pycnocline nutrient concentrations remained elevated suggesting phytoplankton descend to utilize deeper nutrient pools. Except for ammonium, depth-averaged nutrient concentrations were larger in CWW under MW than in RWW under CSW (Table 1). These differences will be discussed using nitrate since it is a limiting nutrient in this region [*Cota et al.*, 1996; *Sakshaug*, 2004; *Tremblay et al.*, 2006; *Popova et al.*, 2010], particularly at the surface when concentrations drop below 1 μmol $kg^{-1}$.

Mean nitrate concentrations in CWW below MW were 8.26 μmol $kg^{-1}$ while in RWW below CSW, they were 2.25 μmol $kg^{-1}$ (Table 1). These differences were also observed in nitrate concentrations within the SCM (Table 2). Nitrate, nitrate silicate, and phosphate concentrations within the SCM were significantly higher where there is MW than CSW. The exception is ammonium, which was the same in both MW and CSW SCM. This indicates that less nutrients were available to SCM phytoplankton where there is CSW. Although nutrient concentrations within CSW SCM were relatively low, they were sufficient to support production of the small phytoplankton cells. Smaller phytoplankton can often survive in regions of lower nutrient concentrations as they have higher surface area to volume ratios, which enhances diffusive nutrient uptake. Maximum chlorophyll concentrations were positively correlated with nitrate concentrations within the SCM ($r = 0.54155$, $p < 0.01$), suggesting the horizontal distribution of nutrients may be one cause of SCM patchiness.

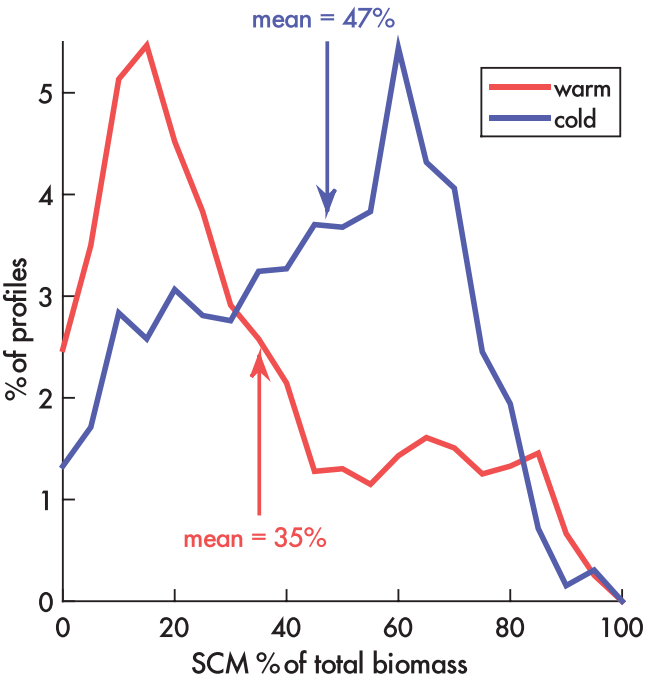


**Figure 9.** Histogram of percent of the total biomass in the SCM from Acrobat data where there is warm CSW (red) and cold MW (blue).

While the nutrient data are too coarse to identify the exact depth of the nutricline (and similarly the nitracline), here we define the depth of the nutricline (and nitracline) to be the depth of the maximum nutrient (and nitrate) gradients determined from the bottle samples. The nitracline deepened as MW was replaced by CSW (Figures 8a and 8b). In most of the profiles, nitrate concentrations were small (<2 μmol $kg^{-1}$) from the surface to below the pycnocline, and then increased between 20 and 30 m (>4 μmol $kg^{-1}$). Other nutrients, ammonium and silicate (Figures 8c and 8f), shared a similar vertical profile with the nutricline

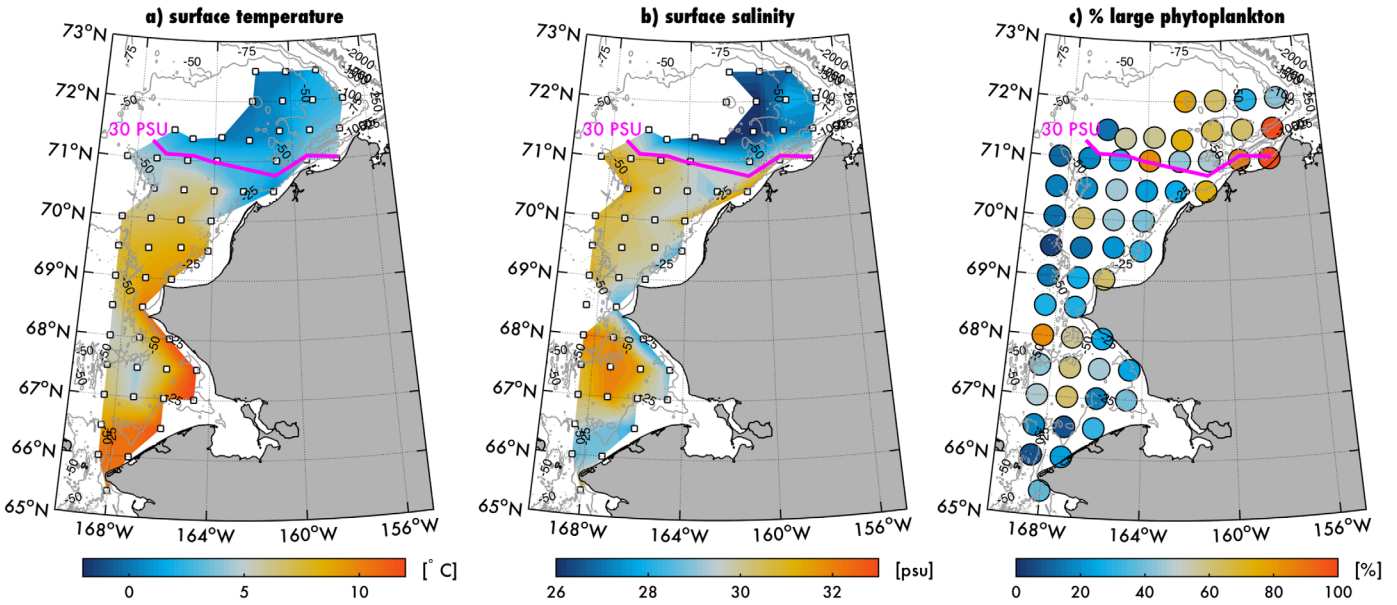


**Figure 10.** Hydrographic and phytoplankton data from the 2013 Arctic Eis cruises. Horizontally interpolated (a) temperature and (b) salinity at 5 m and (c) percent large phytoplankton, where red indicates a higher percentage of large phytoplankton. In each plot, the 30 PSU isohaline (magenta line) is the approximate location of the CSW/MW front.

located below the pycnocline. Oxygen maxima were associated with the pycnocline and found above the depth of the SCM.

Under MW, the SCM was usually found at or below the nutricline (Figure 8h) indicating that SCM depth in CWW is determined by nutricline depth, consistent with other studies [*Brown et al*., 2015; *Lowry et al*., 2015]. The relationship was not as clear where there was CSW, but the limited data suggest that the CSW SCM is more likely to be found above the nutricline (Figure 8g). This is supported by the Acrobat data, where the CSW SCM was found at the pycnocline, above the nutricline as suggested by the shipboard data.

The maximum depth of the SCM is limited by the availability of light. To be consistent with other studies [e.g., *Hill et al*., 2005; *Ardyna et al*., 2013; *Brown et al*., 2015; *Coupel et al*., 2015], the euphotic depth is defined here to be the depth where irradiance is 1% of the surface irradiance. Euphotic depths were relatively constant ranging from 28 to 40 m (Figures 4f, 8g, and 8h) and mean euphotic depths under MW or CSW were not statistically different. The relatively small variation in euphotic depth can be attributed to the lack of light-blocking particulates (phytoplankton, sediment, and CDOM) in the upper layer (Figure 2). Within the depth range at which the SCM was found, irradiance ranged from 0.4 to 10% of surface values. Mean PAR values within the CSW SCM were 8.9% of surface irradiance, or 160% larger than PAR values (3.3%) within the MW SCM. The CSW SCM may remain above the nutricline because low nutrient concentrations in the bottom RWW layer may be insufficient to balance light loss if phytoplankton were to descend.

The sensitivity of the SCM to turbidity and light is also seen in the Acrobat data (Figure 2 and other transects not shown), where the SCM sits above a layer of high particle concentration and CDOM in the bottom layer. This is particularly noticeable north of 71.4°N, where the SCM sits directly above the turbid bottom layer. Between 71.5°N and 71.7°N, patches of higher chlorophyll *a* concentrations near the bottom may be the signature of phytoplankton sinking rather than vertical mixing as turbidity has not increased above the bottom layer.

### 3.5. Phytoplanton Biomass

Chlorophyll *a* fluorescence observed within the SCM was sensitive to changes in hydrography (Figure 2 and Table 1) and suggests phytoplankton biomass will also change as MW is replaced annually by CSW. Although the biomass within the SCM constituted a considerable fraction of the total biomass under both water masses (39%), the percentage of the total biomass that was contained within the SCM was on average higher where there was MW (46%) than CSW (31%) (Figure 9).

The significant contribution of the SCM to the total water column biomass has important implications for the estimation of phytoplankton biomass and primary production from satellite remote sensing data. Due to the shallow penetration depths of these sensors, deeper SCMs are not accounted for in most satellite-based estimates, although attempts have been made to parameterize their contribution [*Uitz et al*., 2006; *Ardyna et al*., 2013]. Because a significant fraction of the total biomass was contained in the SCM, particularly under MW, satellite-based techniques likely underestimate biomass and primary production [*Tremblay et al*., 2008]. *Popova et al*. [2010] finds the SCM contributes 13–46% of the water column-integrated chlorophyll *a* in the Chukchi and if not taken into account can reduce satellite-based estimates by a factor of 3–5 in the euphotic zone [*Martin et al*., 2010]. *Ardyna et al*. [2013] suggests that total primary production estimated from satellite data on Arctic Shelves (<50 m) is underestimated by 15–30% in the post bloom period because of the SCM. Removal of the SCM decreased integrated primary production by 40–70% in satellite-based estimates by *Hill et al*. [2013]. These numbers might be a lower bound, as Acrobat estimates suggest 17–67% of the total biomass is contained within the SCM.

### 3.6. Phytoplankton Community Structure and Ecosystem Dynamics

Seasonal changes in water masses influence phytoplankton biomass, community structure, and the ecosystem of the northeastern Chukchi Sea as a whole. Size-fractionated chlorophyll *a* samples taken during the Arctic Eis cruise indicate that phytoplankton size is sensitive to changes in the upper layer water mass (Figure 10). There was a higher fraction of large phytoplankton in colder MW/CWW than warmer CSW/RWW, the average percent of phytoplankton greater than 10 μm in each region was $62 \pm 7\%$ and $30 \pm 18\%$, respectively.

Differences in phytoplankton size in the northeastern Chukchi indicate the phytoplankton community structure likely changed in response to seasonal hydrographic changes. Higher fractions of large phytoplankton suggest diatoms dominated the MW phytoplankton community, while higher fractions of small phytoplankton suggest picoplankton dominated CSW phytoplankton community. Larger silicate concentrations within the MW SCM support the growth of large phytoplankton such as diatoms, which need silicate to build frustules (Figure 4j and Table 2). A similar relationship between small phytoplankton size and water masses was found when comparing Arctic Eis data from 2012 and 2013 (Danielson et al., submitted manuscript, 2016). Mean water mass temperatures for MW, CSW, and WW were higher and smaller phytoplankton made up more of the biomass in 2012 than in 2013.

Zooplankton communities and species are tied to the different water masses [*Hopcroft et al*., 2010; *Eisner et al*., 2013; *Ershova et al*., 2015], suggesting seasonal changes in hydrography affect all trophic levels in the Chukchi. *Ershova et al*. [2015] found that zooplankton taxa associated with Arctic populations (e.g., copepods *Metridia longa* and *Jaschnovia* spp.) were found in greater abundance in WW, while those associated with Bering Sea populations (e.g., copepods *Pseudocalanus* spp., *Oithona similis*, *Calanus glacialis*, *Metridia pacifica*, and *Euclanus bungii*) were found in greater abundance in warmer Pacific water advected northward from the Bering Strait. In the Chukchi Sea, there was also twice the zooplankton biomass and abundance during the cold summers of 2009–2012 than the warmer summer of 2004. It is unclear whether these changes at different trophic levels are linked and how they affect ecosystems as a whole. Do changes at lower trophic levels cascade to higher ones, e.g., when MW is replaced with CSW and there is less prey available does zooplankton abundance change? Or are the changes at each trophic level independent, e.g., is the MW trophic structure simply replaced with a CSW trophic structure?

## 4. Summary and Conclusions

After the spring bloom when nutrients in the surface are depleted in the northeastern Chukchi Sea (nitrate $< 1$ μmol kg$^{-1}$, nitrite $< 0.1$ μmol kg$^{-1}$, ammonium $< 1$ μmol kg$^{-1}$, and silicate $< 10$ μmol kg$^{-1}$), phytoplankton utilize deeper nutrient pools forming subsurface chlorophyll *a* maxima that persist until the late summer. Using a high-resolution towed instrument platform, we quantify thickness (1–30 m) and for the first time the size (150 m to >45 km long) of the SCM patches, which are typically smaller than the resolution of shipboard surveys. The characteristics of the SCM are dependent on seasonal changes in hydrography in the northern Chukchi Sea. Colder, fresher MW is replaced by northward flowing warmer, saltier CSW that has lower nutrient concentrations, and the SCM becomes shallower and thinner. The MW SCM account for the majority of the total local biomass, while the CSW SCM account for less than half. Larger

phytoplankton are found in MW, where high silicic acid concentrations favor diatom growth, while smaller phytoplankton dominate CSW where silicic acid concentrations are low.

The high-resolution surveys show that SCMs are important contributors to the net phytoplankton biomass in the northeastern Chukchi Sea in late summer. Similar to previous studies [*Tremblay et al*., 2008; *Martin et al*., 2010; *Popova et al*., 2010; *Ardyna et al*., 2013; *Hill et al*., 2013], these observations suggest biomass and primary production estimates are underestimated when the contribution of the SCM which is not resolved by ocean color satellites is not considered. Seasonal cycles of phytoplankton biomass are also likely to change with accelerating Arctic sea ice decline [*Comiso et al*., 2008] and earlier onset of sea ice melt [*Markus et al*., 2009; *Stroeve et al*., 2014]. Earlier ice melt leads to earlier replacement of MW by CSW and could cause decreased phytoplankton biomass and size in late summer. Similar changes at higher trophic levels associated with different water masses suggest that these changes in seasonal water masses affect multiple trophic levels and must be taken into account when exploring ecosystem dynamics in the Chukchi Sea.

**Acknowledgments**

Thanks go to the captains, crews, and scientists aboard the R/V Aquila (ARCWEST), the Bering Explorer (Arctic Eis), and R/V Norseman II. Arctic Eis was funded under grants including the Coastal Impact Assistance Program (USFWS) Agreement Number F12AF00188 and the Bureau of Ocean Energy Management (BOEM), and Environmental Studies Program Agreement Numbers M12AC00009, M12PG00018, and M10PG00050. ARCWEST was funded by the Bureau of Ocean Energy Management under Inter-Agency Agreement Number M12PG00021. The Acrobat data sets used in this paper were supported by BOEM Environmental Studies Program (AK-12-03a) and are archived with the authors and with NODC, the Alaska Ocean Observing System (AOOS), and BOEM. This research is contribution EcoFOCI-0858 to NOAA's Ecosystems and Fisheries-Oceanography Coordinated Investigations, PMEL contribution 4385. This publication is partially funded by the Joint Institute for the Study of the Atmosphere and Ocean (JISAO) under NOAA Cooperative Agreement NA10OAR4320148, Contribution 2469. The authors would like to thank three anonymous reviewers whose suggestions greatly improved this manuscript.

## References

Ardyna, M., M. Babin, M. Gosselin, E. Devred, S. Bélanger, A. Matsuoka, and J.-E. Tremblay (2013), Parameterization of vertical chlorophyll a in the Arctic Ocean: Impact of the subsurface chlorophyll maximum on regional, seasonal, and annual primary production estimates, *Biogeosciences*, *10*(6), 4383–4404, doi:10.5194/bg-10-4383-2013.

Arrigo, K. R., and G. L. van Dijken (2011), Secular trends in Arctic Ocean net primary production, *J. Geophys. Res.*, *116*, C09011, doi:10.1029/2011JC007151.

Arrigo, K. R., G. van Dijken, and S. Pabi (2008), Impact of a shrinking Arctic ice cover on marine primary production, *Geophys. Res. Lett.*, *35*, L19603, doi:10.1029/2008GL035028.

Arrigo, K. R., et al. (2012), Massive phytoplankton blooms under Arctic sea ice, *Science*, *336*(6087), 1408, doi:10.1126/science.1215065.

Belanger, S., M. Babin, and J.-E. Tremblay (2013), Increasing cloudiness in arctic damps the increase in phytoplankton primary production due to sea ice receding, *Biogeosciences*, *10*(6), 4087–4101, doi:10.5194/bg-10-4087-2013.

Brown, Z. W., K. E. Lowry, M. A. Palmer, G. L. van Dijken, M. M. Mills, R. S. Pickart, and K. R. Arrigo (2015), Characterizing the subsurface chlorophyll a maximum in the Chukchi Sea and Canada Basin, *Deep Sea Res., Part II*, *118*, 88–54, doi:10.1016/j.dsr2.2015.02.010.

Brugler, E. T., R. S. Pickart, G. Moore, S. Roberts, T. J. Weingartner, and H. Statscewich (2014), Seasonal to interannual variability of the Pacific water boundary current in the Beaufort Sea, *Prog. Oceanogr.*, *127*, 1–20, doi:10.1016/j.pocean.2014.05.002.

Carmack, E., and D. C. Chapman (2003), Wind-driven shelf/basin exchange on an Arctic shelf: The joint roles of ice cover extent and shelf-break bathymetry, *Geophys. Res. Lett.*, *30*(14), 1778, doi:10.1029/2003GL017526.

Coachman, L. K., and K. Aagaard (1966), On the water exchange through Bering Strait, *Limnol. Oceanogr.*, *11*(1), 44–59, doi:10.4319/lo.1966.11.1.0044.

Coachman, L. K., K. Aagaard, and R. B. Tripp (1975), *Bering Strait: The Regional Physical Oceanography*, Univ. of Wash. Press, Seattle, Wash.

Codispoti, L., C. Flagg, V. Kelly, and J. H. Swift (2005), Hydrographic conditions during the 2002 SBI process experiments, *Deep Sea Res., Part II*, *52*(24–26), 3199–3226, doi:10.1016/j.dsr2.2005.10.007.

Codispoti, L., C. Flagg, and J. H. Swift (2009), Hydrographic conditions during the 2004 SBI process experiments, *Deep Sea Research Part II: Topical Studies in Oceanography*, *56*(17), 1144–1163, doi:10.1016/j.dsr2.2008.10.013.

Comiso, J. C., C. L. Parkinson, R. Gersten, and L. Stock (2008), Accelerated decline in the Arctic sea ice cover, *Geophys. Res. Lett.*, *35*, L01703, doi:10.1029/2007GL031972.

Cooper, L. W., G. F. Cota, L. R. Pomeroy, J. M. Grebmeier, and T. E. Whitledge (1999), Modification of NO, PO, and NO/PO during flow across the Bering and Chukchi shelves: Implications for use as Arctic water mass tracers, *J. Geophys. Res.*, *104*(C4), 7827–7836, doi:10.1029/1999JC900010.

Cota, G., L. Pomeroy, W. Harrison, E. Jones, F. Peters, W. Sheldon Jr., and T. Weingartner (1996), Nutrients, primary production and microbial heterotrophy in the southeastern Chukchi Sea: Arctic summer nutrient depletion and heterotrophy, *Mar. Ecol. Prog. Ser.*, *135*(1), 247–258.

Coupel, P., D. Ruiz-Pino, M. Sicre, J. Chen, S. Lee, N. Schiffrine, H. Li, and J. Gascard (2015), The impact of freshening on phytoplankton production in the Pacific Arctic Ocean, *Prog. Oceanogr.*, *131*, 113–125, doi:10.1016/j.pocean.2014.12.003.

Eisner, L., N. Hillgruber, E. Martinson, and J. Maselko (2013), Pelagic fish and zooplankton species assemblages in relation to water mass characteristics in the northern Bering and southeast Chukchi seas, *Polar Biol.*, *36*(1), 87–113.

Ershova, E., R. Hopcroft, and K. Kosobokova (2015), Inter-annual variability of summer mesozooplankton communities of the western Chukchi Sea: 2004–2012, *Polar Biol.*, *38*(9), 1461–1481.

Gong, D., and R. S. Pickart (2015), Summertime circulation in the eastern Chukchi Sea, *Deep Sea Res., Part II, 118, Part A*, 18–31, doi:10.1016/j.dsr2.2015.02.006.

Gordon, L. I., J. C. Jennings, A. A. Ross Jr., and J. M. Krest (1994), A suggested protocol for continuous flow automated analysis of seawater nutrients (phosphate, nitrate, nitrite and silicic acid) in the WOCE Hydrographic Program and the Joint Global Ocean Fluxes Study, in *WOCE Operations Manual, vol. 3, The Observational Program, Section 3.1, WOCE Hydrographic Program, Part 3.1.3, WHP Operations and Methods*, 55 pp., Woods Hole, Mass.

Grebmeier, J. M., L. W. Cooper, H. M. Feder, and B. I. Sirenko (2006), Ecosystem dynamics of the Pacific-influenced Northern Bering and Chukchi Seas in the Amerasian Arctic, *Prog. Oceanogr.*, *71*(2–4), 331–361, doi:10.1016/j.pocean.2006.10.001.

Hill, V., and G. Cota (2005), Spatial patterns of primary production on the shelf, slope and basin of the Western Arctic in 2002, *Deep Sea Res., Part II*, *52*, 3344–3354.

Hill, V., G. Cota, and D. Stockwell (2005), Spring and summer phytoplankton communities in the Chukchi and Eastern Beaufort Seas, *Deep Sea Res., Part II*, *52*(24–26), 3369–3385, doi:10.1016/j.dsr2.2005.10.010.

Hill, V. J., P. A. Matrai, E. Olson, S. Suttles, M. Steele, L. Codispoti, and R. C. Zim-merman (2013), Synthesis of integrated primary production in the Arctic Ocean: II. In situ and remotely sensed estimates, *Prog. Oceanogr.*, *110*, 107–125, doi:10.1016/j.pocean.2012.11.005.

Hopcroft, R. R., K. N. Kosobokova, and A. I. Pinchuk (2010), Zooplankton community patterns in the Chukchi Sea during summer 2004, *Deep Sea Res., Part II*, *57* (1–2), 27–39, doi:10.1016/j.dsr2.2009.08.003.

Johnson, G. C., J. M. Toole, and N. G. Larson (2007), Sensor corrections for Sea-Bird SBE-41CP and SBE-41 CTDs, *J. Atmos. Oceanic Technol.*, *24*(6), 1117–1130, doi:10.1175/JTECH2016.1.

Lowry, K. E., R. S. Pickart, M. M. Mills, Z. W. Brown, G. L. van Dijken, N. R. Bates, and K. R. Arrigo (2015), The influence of winter water on phytoplankton blooms in the Chukchi Sea, *Deep Sea Res., Part II*, *118*, Part A, 53–72, doi:10.1016/j.dsr2.2015.06.006.

Lu, K., T. Weingartner, S. Danielson, P. Winsor, E. Dobbins, K. Martini, and H. Statscewich (2015), Lateral mixing across ice meltwater fronts of the Chukchi Sea shelf, *Geophys. Res. Lett.*, *42* 6754–6761, doi:10.1002/2015GL064967.

Markus, T., J. C. Stroeve, and J. Miller (2009), Recent changes in Arctic sea ice melt onset, freezeup, and melt season length, *J. Geophys. Res.*, *114*, C12024, doi:10.1029/2009JC005436.

Martin, J., J.-É. Tremblay, J. Gagnon, G. Tremblay, A. Lapoussière, C. Jose, M. Poulin, M. Gosselin, Y. Gratton, and C. Michel (2010), Prevalence, structure and properties of subsurface chlorophyll maxima in Canadian Arctic waters, *Mar. Ecol. Prog. Ser.*, *412*, 69–84.

McLaughlin, F. A., and E. C. Carmack (2010), Deepening of the nutricline and chlorophyll maximum in the Canada Basin interior, 2003–2009, *Geophys. Res. Lett.*, *37*, L24602, doi:10.1029/2010GL045459.

Pabi, S., G. L. van Dijken, and K. R. Arrigo (2008), Primary production in the Arctic Ocean, 1998–2006, *J. Geophys. Res.*, *113*, C08005, doi:10.1029/2007JC004578.

Paquette, R. G., and R. H. Bourke (1974), Observations on coastal current of Arctic Alaska, *J. Mar. Res.*, *32*(2), 195–207.

Paquette, R. G., and R. H. Bourke (1981), Ocean circulation and fronts as related to ice melt-back in the Chukchi Sea, *J. Geophys. Res.*, *86*(C5), 4215–4230, doi:10.1029/JC086iC05p04215.

Parsons, T. R., Y. Maita, and C. M. Lalli (1984), *A Manual of Biological and Chemical Methods for Seawater Analysis*, Pergamon, Oxford, U. K.

Pickart, R. S., L. M. Schulze, G. Moore, M. A. Charette, K. R. Arrigo, G. van Dijken, and S. L. Danielson (2013), Long-term trends of upwelling and impacts on primary productivity in the Alaskan Beaufort Sea, *Deep Sea Res., Part I*, *79*, 106–121, doi:10.1016/j.dsr.2013.05.003.

Popova, E. E., A. Yool, A. C. Coward, Y. K. Aksenov, S. G. Alderson, B. A. de Cuevas, and T. R. Anderson (2010), Control of primary production in the arctic by nutrients and light: Insights from a high resolution ocean general circulation model, *Biogeosciences*, *7*(11), 3569–3591, doi:10.5194/bg-7-3569-2010.

Questel, J. M., C. Clarke, and R. R. Hopcroft (2013), Seasonal and interannual variation in the planktonic communities of the northeastern Chukchi Sea during the summer and early fall, *Cont. Shelf Res.*, *67*, 23–41, doi:10.1016/j.csr.2012.11.003.

Sakshaug, E. (2004), *Primary and Secondary Production in the Arctic Seas*, pp. 57–81, Springer, Berlin.

Stigebrandt, A. (1984), The North Pacific: A global-scale estuary, *J. Phys. Oceanogr.*, *14*(2), 464–470, doi:10.1175/1520-0485(1984)014 < 0464:TNPAGS>2.0.CO;2.

Stroeve, J. C., T. Markus, L. Boisvert, J. Miller, and A. Barrett (2014), Changes in Arctic melt season and implications for sea ice loss, *Geophys. Res. Lett.*, *41*, 1216–1225, doi:10.1002/2013GL058951.

Tremblay, J.-É., C. Michel, K. A. Hobson, M. Gosselin, and N. M. Price (2006), Bloom dynamics in early opening waters of the Arctic Ocean, *Limnol. Oceanogr.*, *51*(2), 900–912, doi:10.4319/lo.2006.51.2.0900.

Tremblay, J.- É., K. Simpson, J. Martin, L. Miller, Y. Gratton, D. Barber, and N. M. Price (2008), Vertical stability and the annual dynamics of nutrients and chlorophyll fluorescence in the coastal, southeast Beaufort Sea, *J. Geophys. Res.*, *113*, C07S90, doi:10.1029/2007JC004547.

Uitz, J., H. Claustre, A. Morel, and S. B. Hooker (2006), Vertical distribution of phyto-plankton communities in open ocean: An assessment based on surface chlorophyll, *J. Geophys. Res.*, *111*, C08005, doi:10.1029/2005JC003207.

Walsh, J., et al. (1989), Carbon and nitrogen cycling within the Bering/Chukchi seas: Source regions for organic matter effecting AOU demands of the Arctic Ocean, *Prog. Oceanogr.*, *22*(4), 277–359, doi:10.1016/0079-6611(89)90006-2.

Wang, J., G. F. Cota, and J. C. Comiso (2005), Phytoplankton in the Beaufort and Chukchi Seas: Distribution, dynamics, and environmental forcing, *Deep Sea Res., Part II*, *52*(24–26), 3355–3368, doi:10.1016/j.dsr2.2005.10.014.

Wassmann, P., and M. Reigstad (2011), Future Arctic Ocean seasonal ice zones and implications for pelagic-benthic coupling, *Oceanography*, *24*(3), 220–231.

Weingartner, T., K. Aagaard, R. Woodgate, S. Danielson, Y. Sasaki, and D. Cavalieri (2005), Circulation on the north central Chukchi Sea shelf, *Deep Sea Res., Part II*, *52*(24–26), 3150–3174, doi:10.1016/j.dsr2.2005.10.015.

Woodgate, R. A., K. Aagaard, and T. J. Weingartner (2005), A year in the physical oceanography of the Chukchi Sea: Moored measurements from Autumn 1990–1991, *Deep Sea Res., Part II*, *52*(24–26), 3116–3149, doi:10.1016/j.dsr2.2005.10.016.

Yun, M. S., T. E. Whitledge, M. Kong, and S. H. Lee (2014), Low primary production in the Chukchi Sea shelf, 2009, *Cont. Shelf Res.*, *76*, 1–11, doi:10.1016/j.csr.2014.01.001.